

# Image Inpainting using Block-wise Procedural Training with Annealed Adversarial Counterpart

Anonymous ECCV submission

Paper ID 1283

**Abstract.** Recent advances in deep generative models have shown promising potential in image inpainting, which is the task of predicting missing pixel values of an image using surrounding context. However, such models are either slow or fail to generate large hole contents. We present a new method for synthesizing high-quality photo-realistic inpaintings from incomplete images using conditional generative adversarial networks (conditional GANs). In particular, we introduce a block-wise procedural training scheme, in conjunction with an annealed adversarial loss, to stabilize the training process of a very deep generative network. We also discuss the effectiveness of a novel patch perceptual loss and multi-scale patch adversarial loss as loss functions. Finally, we extend our framework to several real-world scenarios, including object removal and guided inpainting. Extensive experiments and user-study show that our method significantly outperforms existing methods in all these tasks.

**Keywords:** deep generative model, image inpainting, image harmonization, image composition.

## 1 Introduction

Image inpainting is the task to fill in the missing part of an image with visually plausible contents. It is one of the most typical operations of image editing [1] and low-level computer vision [2, 3]. The goal of image inpainting is to create semantically plausible contents with rich texture details, which can either be consistent with the original contents or is coherent with the known context such that the output image appears realistic. Other than image restoring and fixing, inpainting can also be used to remove unwanted objects, or in the case of guided inpainting, it can be used to composite with the contents from another image. In the latter scenario, we often need harmonization to adjust the appearance of the guidance image to make it compatible with the known context. Meanwhile, inpainting is needed to fill in the gaps between the two images.

Traditional image inpainting methods mostly develop texture synthesis techniques to address the problem of hole-filling [4, 2, 5–8]. In [6], Barnes et al. proposes the Patch-Match algorithm which efficiently searches for the most similar patch to reconstruct the missing regions. Wilczkowiak et al. [8] takes further steps and detects desirable search regions to find better match patches. However,

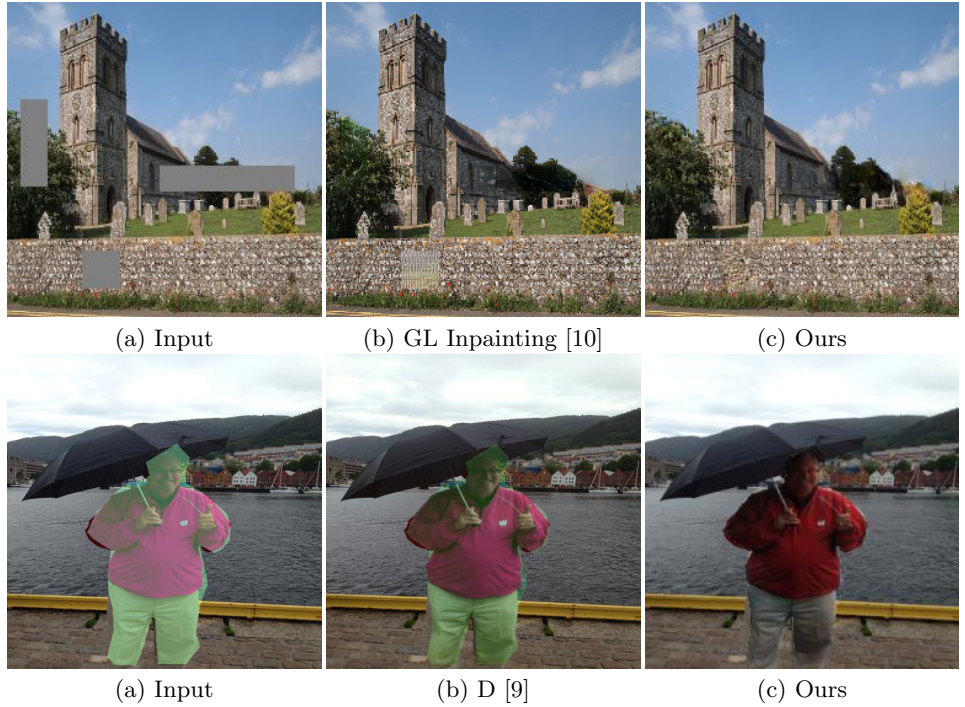


**Fig. 1.** An example result of inpainting (top) and harmonization (bottom). As a general image translation framework, our approach outperforms state-of-the-art methods in both tasks (zoom in for best view). Combining inpainting and harmonization we can easily achieve image composition and guided inpainting (Sec. 4.4).

these methods only exploit the low-level signal of the known contexts to hallucinate missing regions and fall short of understanding and predicting high-level semantics. Furthermore, it is often challenging to capture the global structure of images by simply extending texture from surrounding regions. Another line of work for inpainting aims to fill in holes with content from another guidance image, by using composition and harmonization [3, 9]. The guidance image is often retrieved from a large database of images before it is pasted blended with the original image. Although these methods are able to propagate high-frequency details from the guidance image, they often introduce inconsistent regions and gaps which are easily detectable with human eyes.

More recently, deep neural networks have exhibited excellent performance in various computer vision tasks, including texture synthesis and image completion. In particular, adversarial training becomes the de facto strategy to train an image inpainting model [11–14, 10]. Pathak et al. [11] first proposes to train an encoder-decoder model to synthesize missing holes from surrounding pixels, using both the reconstruction loss and the adversarial loss. In [12], Yeh et al. addresses inpainting by using a pre-trained model to find the most similar encoding of the corrupted image. Yang et al. [14] proposes a multi-scale neural patch synthesis

approach, which optimizes the hole contents such that its feature extracted from middle layers of a pre-trained CNN matches with the features of the surrounding context. The optimization greatly improves the inpainting quality and resolution at the cost of computational efficiency. Iizuka et al. [10] instead proposes a pure feed-forward model trained with global and local GANs, and generates excellent results for small holes. However, DNN based methods have several limitations. First, they are either too slow due to optimization [14] or cannot generate sufficient high-frequency details, especially for large holes [10]. Second, it is difficult to handle perceptual continuity, making it necessary to resort to post-processing (e.g. Poisson blending for [10]) to smooth out the coalescing regions.

In practice, we found that directly training a very deep generative network to synthesize high-frequency details is difficult. Most often we fail to stabilize the training process and the results are either overly smooth or containing significant noise and artifacts. To overcome this limitation, we discuss a new approach that produces high-quality inpainting results for various inpainting tasks, refer to as **Block-wise Trained Generative Model for Inpainting** (BTGMI). More specifically, we decompose the generator into a ResNet head followed by multiple refinement residual blocks. For the first phase, we train the **ResNet head** for inpainting until it converges. Then we add residual blocks one at a time. Each time we train with an additional block, we use skip connections to initialize with the trained network and gradually increase the weight of the new block. This introduces the new block gradually, forcing it to refine from the previous results and learn to generate richer details. In addition, we observe that it is essential to steadily reduce the weight of the generator adversarial loss during block-wise refinement. We refer to this training scheme as **Adversarial Loss Annealing** (ALA). Intuitively, AAL is helpful as the adversarial loss usually dominates in the end phase of training and the generator will falsely create noise patterns to foul the discriminator. Finally, Zhang et al. [15] shows that the perceptual similarity, measured by internal activations of networks trained for high-level classification tasks, corresponds to human perceptual judgment far better than commonly used metrics such as the Euclidean distance. Inspired by this finding, we introduce a novel **Patch Perceptual Loss** (PPL), which penalize the perceptual difference between the inpainted patch and the original patch. Different from the perceptual losses ,used in style transfer [16, 17] and image synthesis [18, 19], we compute the feature disparity across all layers. In our experiment, we found that PPL works better than the reconstruction loss and the general perceptual loss.

To evaluate the proposed inpainting approach, we conduct extensive experiments on different datasets. We also show that our model, although being designed for inpainting, can be used for general image translation tasks including image harmonization and composition. This enables us to jointly train inpainting with those tasks and makes it suitable for a wide range of inpainting scenarios such as object removal and guided inpainting. As shown by visual results and user-study, our network already outperforms state-of-the-art inpainting and harmonization methods without using block-wise refinement. By leveraging block-wise training, it can further add high-frequency details and eliminate the

135 perceptual discontinuity (Fig. 1). Finally, we demonstrate our approach is both  
 136 effective and simple to use in several real-world use cases.

137 In summary, in this paper we present:

- 138 1. The Block-wise Trained Generative Model for Inpainting (BTGMI) as a  
 139 novel, end-to-end model that generates state-of-the-art image inpainting and  
 140 image composition results.
- 141 2. Two novel training losses specifically designed for the inpainting task: the  
 142 Patch Perceptual Loss (PPL) and the Multi-Scale Patch Adversarial Loss  
 143 (MSPAL). We also introduce Adversarial Loss Annealing (ALA) as a new  
 144 training scheme that improves the inpainting quality.
- 145 3. Effectiveness of our approach in practical use cases, including distractor re-  
 146 moval and guided inpainting.

## 149 2 Related Work

150 **Deep image generation and manipulation** Generative Adversarial Network (GAN) [20] uses a mini-max two-player game to alternatively train a  
 151 generator and a discriminator, and has shown impressive capacity to generate  
 152 natural and high-quality images. However, for the vanilla GANs, the training  
 153 instability makes it hard to scale to higher resolution images. Several tech-  
 154 niques have been proposed to stabilize the training process, including Laplacian  
 155 pyramid GAN [21], DCGAN [22], energy-based GAN [23], Wasserstein GAN  
 156 (WGAN) [24], WGAN-GP [25] and the Progressive GAN [26]. Both BTGMI and  
 157 Progressive GAN gradually increase the depth of the network during training.  
 158 While Progressive GAN addresses the image synthesis problem, our architecture  
 159 poses as an ideal candidate for image translation tasks. A major model difference  
 160 between BTGMI and Progressive GAN is that, rather than bringing in convolu-  
 161 tional layers at the end of the network, we progressively insert residual blocks  
 162 before the upsampling layers.

163 Adversarial training, as a general idea for DNN based methods, has been  
 164 widely applied to various research fields, especially many image editing tasks  
 165 such as image super-resolution [27–29], image-to-image translation [30, 31], im-  
 166 age inpainting and image harmonization. Recently, [32] proposes the Pix2Pix HD  
 167 model for high-resolution image synthesis using conditional GANs, which pro-  
 168 duces very high-quality simulated images from semantic maps, human sketches,  
 169 etc. Our ResNet head simplifies the Pix2Pix HD model and also improves the  
 170 synthesis quality by re-designing its losses. For the image inpainting task, many  
 171 DNN based approaches achieve good performance by different network topology  
 172 and training procedure [11, 14, 12, 10]. Image harmonization, on the other hand,  
 173 aims to adjust the appearances of the foreground and background regions such  
 174 that they are compatible and the composition is realistic. In [33], Zhu et al.  
 175 trains a CNN model to measure how realistic of a composite image is, and uses  
 176 this metric to adjust and optimize the appearance of the foreground region. Tsai  
 177 et al. [9] also proposes a DNN based method by training a deep CNN to learn

and predict the context and semantic information of composite images. However, the limitation of image harmonization alone is that low-level appearance or color adjustments are often inadequate to make the composition realistic. In contrast, our approach of guided inpainting not only adjusts the appearance of the guidance patch, but also synthesizes new contents to fill in the gaps and smoothes the transition between the foreground and the background.

**Non-neural image inpainting and harmonization** Traditional image completion algorithms can be either diffusion-based [4, 34] or patch-based [7, 6]. Diffusion-based methods usually cannot synthesize plausible contents for large holes or textures, due to the fact that it only propagates low-level features. Patch-based methods, however, largely rely on the assumption that the desired patches exist in the database. For harmonization, traditional methods usually apply color and tone matching, by matching global statistics [35] or multi-scale statistics [36], extracting gradient domain information [37, 38], or utilizing semantic clues [39]. [40] further develops a data-driven method, which searches and retrieves multiple real images with similar structural layouts and use them to transfer the appearances. A complete comparison with non-neural inpainting and harmonization algorithms is beyond the scope of our paper.

### 3 Our Method

In this section, we describe our model and several training schemes. First, we illustrate the details of our basic components: the generator head and the training losses, in Sec. 3.1. Then, we describe the block-wise procedural training scheme and the adversarial loss annealing in Sec. 3.3. Finally, we summarize our implementation and training details.

Our generator head is a conditional GAN network [41], which takes an incomplete image as the input, and outputs a complete image. Conditional GANs for image inpainting usually consist of a generator  $G$  and a discriminator  $D$ . The generator  $G$  learns to predict the hole contents and restore the complete image, while the discriminator  $D$  learns to distinguish real images from the generated ones. The model is trained in a self-supervised manner via the following minimax game:

$$\min_G \max_D E_{(s,x)}[\log D(s, x)] + E_s[\log(1 - D(s, G(s)))] \quad (1)$$

where  $s$  and  $x$  are the incomplete image and the original image respectively, and  $G(s)$  is the generator prediction given the input  $s$ . Note that if  $G(s)$  predicts an entire image as output, we only keep the hole contents and concatenate with the known context of  $s$ .

#### 3.1 The Generator Head

Previous research experimented with different architecture of  $G$ , most notably the U-Net style generator of [11] and the FCN style generator of [10]. [10] shows

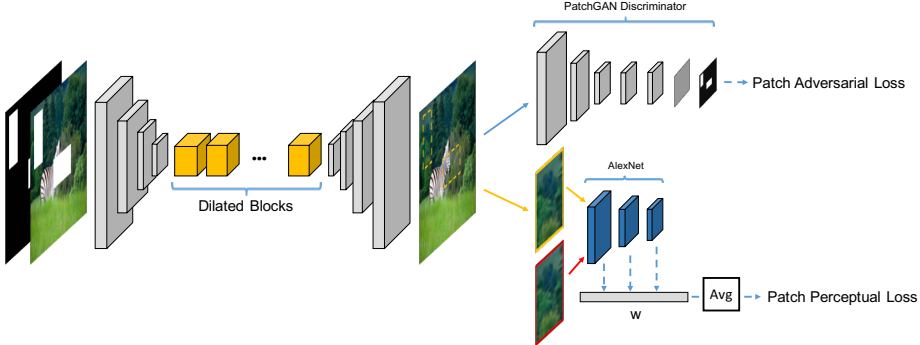


**Fig. 2.** Generator head and the training losses. We only illustrate one scale of Patch Adversarial Loss and Patch Perceptual Loss. Note that to compute the Patch Adversarial Loss, we need to use the mask to find out which patch overlaps with the hole.

that FCN style inpainting network produces less blurred results than U-Net, as it adopts fully convolutional layers instead of an intermediate fully connected (FC) layer, which avoids significant resolution reduction or information loss.

Similar to [10], our generator head is based on FCN and leverage the many properties of convolutional neural networks, including translation invariance and parameter sharing. Nevertheless, a major limitation of FCN is the constraint of the receptive field size, since the convolution layers are locally connected, making pixels far away from the hole carry no influence on the predicted hole content. We rely on several strategies to alleviate such drawback. First, like [10], we use a down-sampling front end to reduce the feature size, followed by multiple residual blocks [42], and then an up-sampling back end to restore the full dimension. By downsampling, we increase the receptive field of the ResNet blocks. Second, we stack multiple ResNet blocks to further enlarge the receptive field. Finally, we adopt the dilated convolutional layers [43] in all ResNet blocks. Dilated convolutions use spaced kernels, making it compute each output value with a wider view of input without increasing the number of parameters and computational burden. We set the dilation factor to 2 in all layers. Overall, we observe context is critical for realism, and the receptive size poses as an important factor for inpainting quality. This differentiates it from other image translation tasks.

Specific to our network, the down-sampling front end consists of three convolutional layers, each with stride 2. The intermediate residual blocks contain 9 blocks stacked together, and the up-sampling back-end consists of three transposed convolution of stride 2. Each convolutional layer is followed by batch normalization (BN) and ReLu as the activation layer, except for the last layer which outputs the image. For down-sampling and up-sampling, an alternative would be using interpolated convolution to reduce the checkerboard effect, as suggested by [44]. The interpolated convolution uses a dimension-preserving convolution layer of stride 1, followed by max pooling or bilinear up-sampling. However, we observed that using interpolated convolution creates overly smooth effects. A detailed ablation study is presented in Sec. 5.

### 270    3.2 The Training Losses

271    Different losses have been used to train an inpainting network. These losses  
 272    can be cast into two categories. The first category, which can be referred to as  
 273    *similarity loss*, is used to measure the similarity between the output and the  
 274    original image. The second category, which we refer to as the *realism loss*, is  
 275    used to measure how realistic-looking the output image is. We summarize the  
 276    losses used in different approaches in Table 1.

Method	Similarity Loss	Realism Loss
Context Encoder [11]	$\ell_2$	Global Adversarial Loss
Global Local Inpainting [10]	$\ell_2$	Global and Local Adversarial Loss
Our Approach	Patch Perceptual Loss (PPL)	Improved Multi-Scale Adversarial Loss

283    **Table 1.** Comparison of training losses in different methods.

285    **Patch Perceptual Loss** As shown in Table 1, using  $\ell_2$  loss for reconstruction  
 286    and measure the disparity between the output and the original image has been  
 287    the default choice of previous inpainting methods. However, it is known that  $\ell_2$   
 288    loss does not correspond well to human perception of visual similarity (Zhang et  
 289    al. [15]). This is because  $\ell_2$  losses wrongly assumes each output pixel is condition-  
 290    ally independent of all others. A well-known issue, for example, is that blurring  
 291    an image leads to small changes in terms of Euclidean distance but causes sig-  
 292    nificant perceptual difference. Recent research suggests that a better metric for  
 293    perceptual similarity is the internal activations of deep convolutional networks,  
 294    usually trained on a high-level image classification task. Such loss is called “per-  
 295    ceptual loss”, and is used in various tasks such as neural style transfer [17], image  
 296    super-resolution [16], and conditional image synthesis [18, 19].

297    Based on this observation, we propose a new “patch perceptual loss” as  
 298    the substitute of the  $\ell_2$  losses. Traditional perceptual loss typically uses VGG-  
 299    Net, and computes the  $\ell_2$  distance of the activations on a few feature layers.  
 300    Recently, [45] specifically trained a patch perceptual network to measure the  
 301    perceptual differences between two image patches based on AlexNet, making it  
 302    an ideal candidate for our task. The patch perceptual network computes the ac-  
 303    tivations across all feature layers and sums up the  $\ell_2$  distances scaled by learned  
 304    weights at each layer. Furthermore, to take into account both the local view and  
 305    the global view of perceptual similarity, we compute PPL at two scales. Local  
 306    PPL considers the local hole patch, while the global PPL slightly zooms out to  
 307    cover a larger contextual area. More formally, our PPL is defined as:

$$309 \quad \sum_{p=1,2} PPL_k(G(s)_p, x_p) = \sum_{k=1,2} \sum_l \frac{1}{H_l W_l} \sum_{h,w} \| w_l^T \odot (\hat{F}(x_p)_h^l - \hat{F}(G(s)_p)_h^k) \|_2^2 \quad (2)$$

312    Here  $p$  refers to the hole patch.  $\hat{F}$  is the AlexNet and  $l$  is the feature layer.  
 313    Ablation study in Sec. 5 shows that PPL gives better inpainting quality than  
 314    both  $\ell_2$  and VGG-based perceptual losses.

**Multi-Scale Patch Adversarial Loss** Adversarial losses are given by trained discriminators to discern whether an image is real or fake. The global adversarial loss of [11] takes the entire image as input and outputs a single real/fake prediction, which does not consider the realism of local patches, especially the holes. The additional local adversarial loss of [10] adds another discriminator specifically for the hole, but it requires the hole to be fixed shape and size during training to fit the discriminator. To consider both the global view and the local view, and to be able to use holes of arbitrary number and shapes, we propose to use PatchGAN discriminators [30] at three scales of image resolutions. The discriminator at each scale is identical, only the input is a differently scaled version of the *entire image*. The PatchGAN discriminator at each scale is a convolutional discriminator which outputs a vector of predictions, where each value corresponds to an image patch. In this way, the discriminators are trained to classify global and local image patches across the image, and also enable us to use random holes and shapes during training. However, directly using PatchGAN is problematic in our case, as for the output restored image, only the patches overlapping with the hole area should be considered fake patches. Therefore when computing the discriminator loss of the restored image, instead of forcing the entire output to be fake, only the patches overlapping with the holes are labeled as fake. More formally, our Patch-wise Adversarial Loss is defined as:

$$\min_G \max_{D_1, D_2, D_3} \sum_{k=1,2,3} L_{GAN}(G, D_k) \quad (3)$$

$$= \sum_{k=1,2,3} E_{(s_k, x_k)}[\log(s_k, x_k)] + E_s[\log(Q - D_k(s_k, G(s_k)))]. \quad (4)$$

Here  $k$  refers to the image scale, and  $Q$  is a patch-wise real/fake vector, based on whether the patch overlaps with the holes. Using multiple GAN discriminators at the same or different image scale has been proposed in unconditional GANs [46] and conditional GANs [32]. Here we extend the design to take into account inpainting hole locations, which is critical in obtaining semantically and locally coherent image completion results.

To summarize, our full objective combines both losses is therefore defined as:

$$\min_G (\max_{D_1, D_2, D_3} \lambda_{Adv} \sum_{k=1,2,3} L_{GAN}(G, D_k)) + \lambda_{PPL} \sum_{k=1,2} PPL_k(G(s)_p, x_p)). \quad (5)$$

We use  $\lambda_{Adv}$  and  $\lambda_{PPL}$  to controls the importance of the two terms. In our experiment, we set  $\lambda_{Adv} = 1$  and  $\lambda_{PPL} = 10$  to begin with. As training progresses, we gradually decrease the weight of  $\lambda_{Adv}$  as explained in Sec. 3.3.

Fig. 2 illustrates the architecture of our generator head and the training losses.

### 3.3 Blockwise Procedural Training with Adversarial Loss Annealing

Our experiments show that using the described generator head and training losses already give inpainting results better than state-of-the-art. However, the

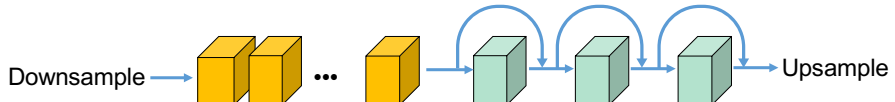


**Fig. 3.** Illustration of block-wise procedural training. The yellow residual blocks refer to the generator head which are trained first. The green residual blocks are progressively added one at a time. We also draw the skip connections between the already trained residual blocks and the up-sampling back end.

results can still lack fine details, especially when synthesizing textures. Result may contain noise patterns when the image is complicated. A straight-forward effort to improve the results would be to stack more intermediate residual blocks to further expand the receptive view and increase the expressiveness of the model. However, we found that directly stacking more residual blocks makes it more difficult to stabilize the training. As the search space becomes much larger, it is also more challenging to find local optimum. In the end, the inpainting quality deteriorates as the model depth increases.

Recently, Progressive GAN [26] was proposed as a new training methodology for generative adversarial networks. The key idea is to grow both the generator and discriminator progressively, by adding new layers that model increasingly fine details as training progresses. This strategy makes the training faster and more stable and enables it to synthesize mega-pixel images with unprecedented visual quality.

We adapt this idea for image inpainting and propose to use procedural block-wise training to gradually increase the depth of the inpainting network. More specifically, we begin by training the generator head until it converges. Then, we add a new residual block after the already trained residual blocks, right before the back-end upsampling layers. In order to smoothly introduce the new residual block without suddenly breaking the trained model, we add another skip path from the trained residual blocks to the upsampling layers. Initially, the weight of the skip path is set to 1, while the weight of the path containing the new block is set to 0. This essentially makes the initial network identical to the already trained network. We then slowly decrease the weight of the skip path and increase the weight of the new residual block as training progresses. In this way, the newly introduced residual block is trained to be a fine-tuning component, which adds another layer of fine details to the original results. This step are repeated multiple times, where each time we expand the model by adding a new residual block. In our experiment, we found that the results improve significantly after fine-tuning with the first additional residual block. The output becomes stabilized after three residual blocks, when little discernible changes can be detected if even more residual blocks are introduced. The procedural training process is illustrated in Fig. 7.

We observe that the block-wise procedural training has several benefits. First, it guides the training process of a very deep generator. Starting with the generator head and gradually fine-tuning with more residual blocks makes it easier to discover the mapping between the incomplete image and the complete im-

age, even though the search space is huge given the diversity of natural images and the random holes. Another benefit is reduced training time, as we found decoupling the training of the generator head and the fine-tuning of additional residual blocks requires significantly less training time comparing with training the network all at once.

**Adversarial Loss Annealing** During training, the generator adversarial loss updates the generator weight if the discriminator successfully detects the generated image as fake:

$$\sum_{k=1,2,3} E_s[\log(\bar{Q} - D_k(s_k, G(s_k)))] \quad (6)$$

Note that here  $\bar{Q}$  reverses  $Q$  of 3.2 as this is the loss to the generator. We observe that the generator adversarial loss becomes dominant over PPL as training progresses. This is because the discriminator becomes increasingly good at detecting fake images during training. This is less of a problem for image synthesis tasks. However, for the inpainting task which requires the output to be faithful to the original image, the outcome is that the generator deliberately adds noise patterns to confuse the discriminators, bringing more artifact to output or even synthesizing wrong textures. Based on this observation, we propose to use adversarial loss annealing, which decreases the weight of the generator adversarial loss when adding new residual block. More formally, let the initial weight of the generator adversarial loss be  $\lambda_{adv}^0$ , and the weight of the generator adversarial loss be  $\lambda_{adv}^i$  after adding the  $i$ th residual block. We found that simply decay the weight linearly by setting  $\lambda_{G_{adv}}^i = 0.1^i \lambda_{G_{adv}}^0$  gives satisfying results. Detailed analysis are described in Sec. 5.

Finally, we summarize the discussed training schemes in Alg. 1.

---

**Algorithm 1** Training the Inpainting Network

---

- 1: Set batch size to 8 and basic learning rate to  $lr_0 \leftarrow 0.0002$ .
  - 2: Set  $\lambda_{PPL} \leftarrow 10$  and  $\lambda_{adv}^0 \leftarrow 1$ .
  - 3: Train the Generator Head  $G_0$  using MSPAL and PPL (3.2) for 150,000 iterations.
  - 4: **for**  $i=1$  to 3 **do**
  - 5:     Add the skip path and the residual block  $r_i$ .
  - 6:     Set  $lr_i \leftarrow 0.1^i lr_0$  and  $\lambda_{G_{adv}}^i \leftarrow 0.1^i \lambda_{G_{adv}}^0$ .
  - 7:     Train the generator  $G_3$  with the added  $r_i$  for 1,500 iterations.
  - 8: **return**  $G_3$
- 

## 4 Results

In this section, we first describe our dataset and experiment setting (Sec. 4.1). We then provide quantitative and qualitative comparisons with several methods, and also report a subjective human perceptual test with user-study (Sec. 4.2).

In Sec. 4.3, we conduct several ablation study about the design choice of the models, losses, and training scheme. Finally, we show how our method can be applied to real use cases of object removal and guided inpainting. In particular, the inpainting model can be adapted to train an image harmonization network, which generates state-of-the-art harmonization results. We then demonstrate that by jointly training a model for inpainting and harmonization we can easily achieve guided inpainting (Sec. 4.4).

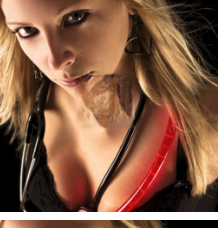
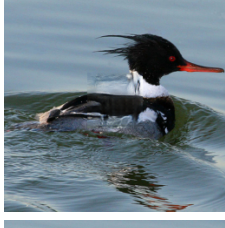
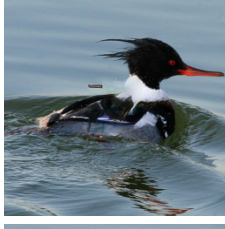
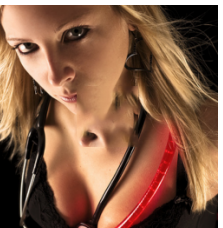
## 4.1 Experiment Setup

We evaluate our inpainting method on several representative datasets. COCO [47] is a large dataset containing both object and scene images; Place2 [48] includes images of a diversity of scenes and was originally meant for scene classification; finally, we train and test on CelebA [49], which consists of 202,599 face images with various viewpoints and expressions. For a fair comparison, we follow the standard split with 162,770 images for training, 19,867 for validation and 19,962 for testing.

In order to compare with existing methods, we train on images of size 256x256. We also train another network at a larger scale of 512x512 to demonstrate its ability to handle higher resolutions and compare with neural patch synthesis [14]. As the pre-processing step, we first resize the image and then conduct random cropping. We then apply data augmentation with random flipping. For each image, we create a mask containing one or two rectangle holes. The size of the hole ranges from 1/4 to 1/2 of the image's dimension, and are positioned at random locations. Note that during inference, our network is able to handle masks with an arbitrary number of holes of any shape. Finally, we shift and rescale the pixel value from [0,255] to [-1,1] and fill in the masked regions with zeros. We then concatenate the corrupted image and the mask as input.

For all our training, we set the learning rate with polynomial decay starting from 0.0002, and adopt Adam for optimization. We set the batch size to 8, and regardless of the actual dataset size, we train 150,000 iterations for the generator head and another 1,500 iterations for each additional residual block. For each dataset, the training takes around 2 days to finish on a single Titan X GPU.





495  
496  
497  
498  
499  
500  
501  
502  
503  
504  
505  
506  
507  
508  
509  
510  
511  
512  
513  
514  
515  
516  
517  
518  
519  
520  
521  
522  
523  
524  
525  
526  
527  
528  
529  
530  
531  
532  
533  
534  
535  
536  
537  
538  
539

540  
541 Table 2: Fixed hole completion comparison. From top row to bot-  
542 tom row: input image, CAF, CE, NPS, GLI and our final results.  
543  
544  
545  
546  
547

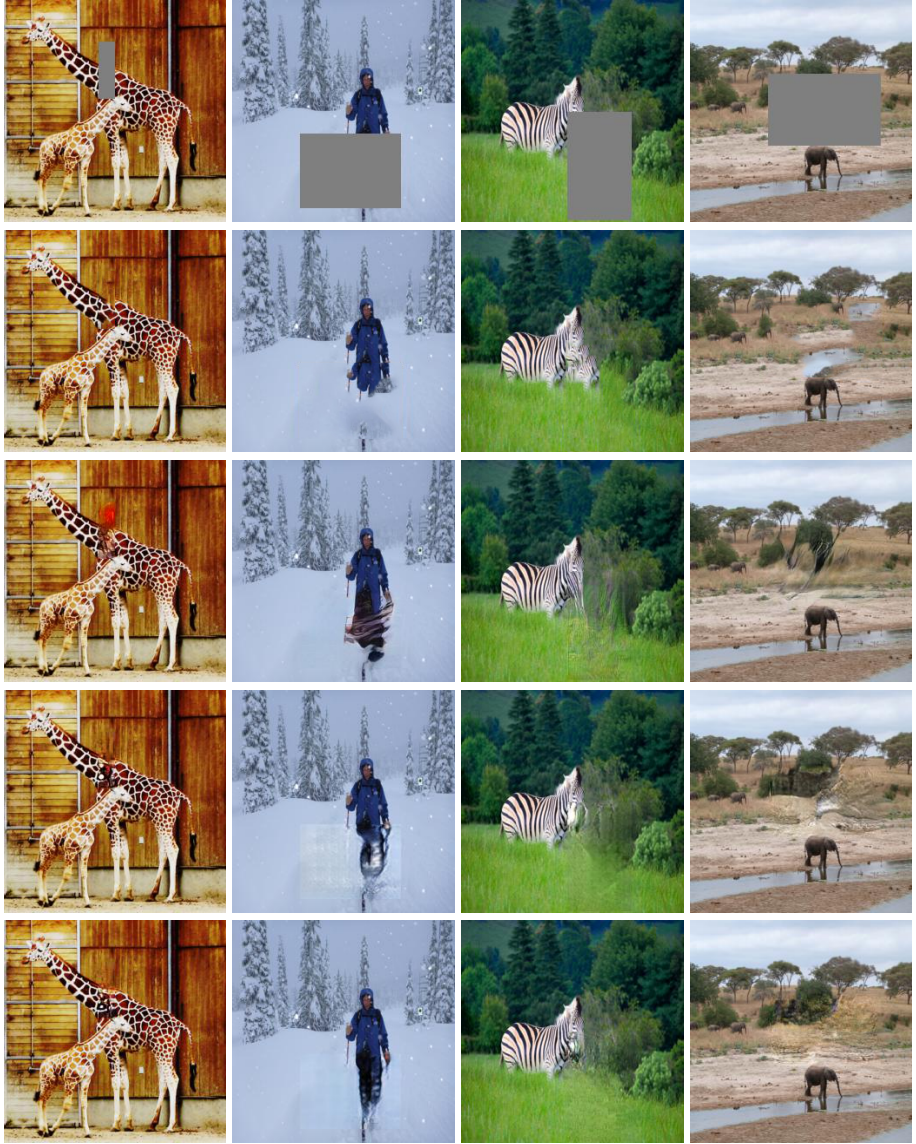


**Fig. 4.** Random hole completion comparison. From top row to bottom row: input image, CAF results, GLI results, our generator head results, our final results.

## 585 4.2 Comparison with Existing Methods

586 At 256x256, we compare our results with Content-Aware Fill (CAF) [6], Con-  
 587 text Encoder (CE) [11], Neural Patch Synthesis (NPS) [14] and Global Local  
 588 Inpainting (GLI) [10]. For CE and GLI, we use off-the-shelf pre-trained models  
 589 from the web. Note CE’s model is trained with center holes and other models are  
 590 able to handle random holes. We evaluate on both settings, using random holes  
 591 (Fig. 4) or center holes (Fig. 4.1). For center hole completion, we compare with  
 592 CAF, CE, NPS and GLI on ImageNet [50] test images. In this case, our results  
 593 are directly generated by models trained on COCO. For random completion, we  
 594 compare with CAF and GLI using images from COCO and Place2. Note GLI’s  
 595 results are after Poisson Blending as post-processing, which other methods do  
 596 not use. For our approach, we show the results generated by the Generator Head  
 597 alone as well as the final results using procedural training as refinement. The  
 598 comparison results shown are randomly sampled from the entire test set.  
 599

600 Based on the visual results we can see that, for CAF as a non-learning and  
 601 patch-based approach, its main issue is the inability to generate novel objects  
 602 not available in the known context. This is especially an issue for highly spe-  
 603 cific and complex structure such as face inpainting. Furthermore, while CAF is  
 604 able to generate realistic-looking details, they do not always capture the global  
 605 structure and the inpainting is often inconsistent when the contexts are com-  
 606 plex. CE’s result is blurrier, and the border between the hole and the context  
 607 is easily detectable. Comparing with NPS, our approach is much faster, as it is  
 608 purely feed-forward while NPS is optimization-based. In fact, NPS takes about  
 609 20 seconds to inpaint an image of 256x256 and 60 seconds for an 512x512 image.  
 610 Our results are also visually better than NPS on 256x256. Comparing with GLI,  
 611 our results do not need fine-tuning, and are less noisy, more coherent, and have  
 612 better quality.

613 For CelebA, we compare with Generative Face Completion [13] in Fig. Since [13]’s  
 614 model inpaints images of 128x128, we have to upsample the results to 256x256  
 615 to compare. The images shown are chosen at random, not cherry-picked. We can  
 616 see that although [13] is a specifically designed model for face inpainting, our  
 617 model generates much better results.

618 **Quantitative Evaluation** Table 3 shows quantitative comparison between  
 619 CAF, CE, GLI and our approach. The values are computed based a random  
 620 subset of 200 images selected from the test set. Both the  $\ell_1$  and  $\ell_2$  errors are  
 621 computed with pixel values normalized between [0, 1] and are summed up using  
 622 all pixels of the image. We can see that our method performs better than other  
 623 methods in terms of SSIM and  $\ell_1$  error. For  $\ell_2$ , other methods have smaller  
 624 errors, possibly due to the fact that our model is trained with perceptual loss  
 625 rather than  $\ell_2$  loss. In addition, from the numerical values, we can see that pro-  
 626 cedural fine-tuning further reduces the error of the generator head. This is also  
 627 validated by qualitative improvements shown in Fig. 4.1 and Fig. 4.

628 **User Study** To more rigorously evaluate the performance, we conduct a user  
 629 study based on the random hole results. We ask 20 users to compare the re-  
 sults, by giving each user 30 image sets to rank the visual quality. Each set

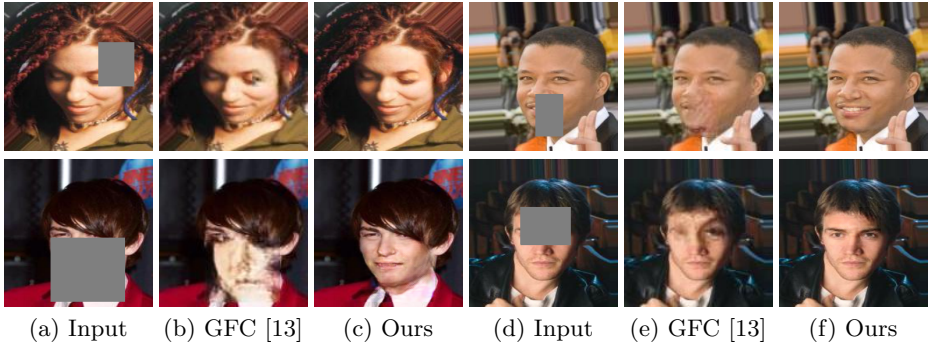


Fig. 5. Face completion results comparing with [13].

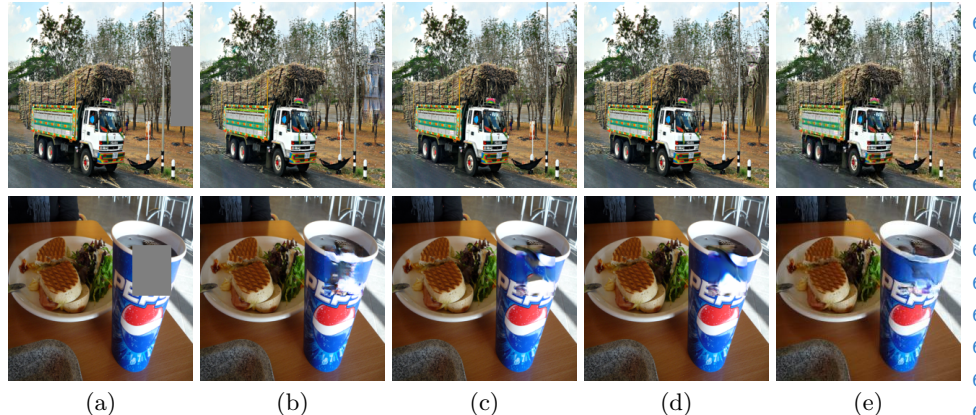
Method	Mean $\ell_1$	Error	Mean $\ell_2$	Error	SSIM
CAF [6]	968.8		<b>209.5</b>		0.9415
	1660		<b>363.5</b>		0.9010
CE [11]	2693		545.8		<b>0.7719</b>
	N/A		N/A		N/A
GLI [10]	868.6		269.7		0.9452
	1640		378.7		0.9020
Ours (Generator Head)	913.8		245.6		0.9458
	1629		439.4		0.9073
Ours (Final)	<b>838.3</b>		253.3		<b>0.9486</b>
	<b>1609</b>		427.0		<b>0.9090</b>

Table 3. Numerical comparison between CAF, CE and GLI, our generator head results and our final results. Up/down are results of center/random region completion. Note that for SSIM, larger values mean greater similarity in terms of content structure and are indicators of better performance.

contains NPS, GLI, and our result respectively. The survey results give convincing evidence that our method works better than other approaches. Among 300 comparisons, 72.3% of the time our results are ranked highest. In particular, our results are overwhelmingly better than NPS, and in 95.8% of the comparisons our results are better. 73.5% of our results are better than GLI, and 15.5% have similar qualities. This shows that our results have significant advantages over GLI, and are also better or comparable with CAF most of the time.

### 4.3 Ablation Study

**Comparison of Convolutional Layer** Choosing the proper convolutional layer improves the inpainting quality and also reduces the noise. We consider three types of convolutional layers: vanilla, dilated [43] and interpolated [44], and train three networks to specifically test the effects of different convolutional layers. Fig. shows an example of qualitative comparisons. We can see that using dilation significantly improve the inpainting quality comparing with vanilla convolutional layer and interpolated convolutional layer, as the latter generates results that are over-smoothed.



**Fig. 6.** Effects of different types of convolutional layers. (a) Input. (b) Vanilla (c) Interpolated (d) Dilated+Interpolated (e) Dilated (ours).

**Effect of Procedural Training** Qualitative comparisons in Sec. 4.2 shows that procedurally adding residual blocks to fine-tune improves the results. However, one may wonder whether we can directly train a deeper network. To find out, we trained the same number of iterations for a network with 12 residual blocks from scratch. Fig. 7 shows two examples of the results of inpainting using the trained model comparing with the results of the block-wise trained model. For all the test images, we found that increasing number of layers actually has a negative effect on inpainting, due to a variety of factors such as gradient vanishing, optimization difficulty, etc. This experiment demonstrates the necessity and importance of the procedural training scheme.

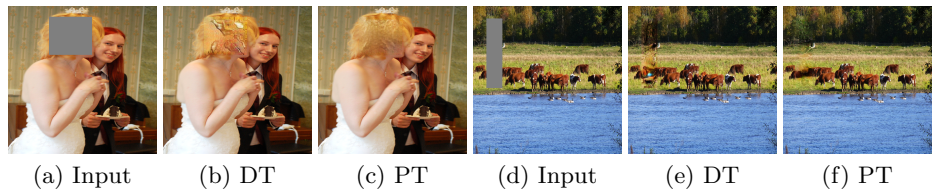


**Fig. 7.** Result comparison between directly training a network of 12 blocks ((b),(e)) and procedural training ((c), (f)).

**Effect of Adversarial Loss Annealing** We investigate the effect of adversarial loss annealing in terms of reducing the noise level. As discussed in Sec. 3.3, the adversarial loss becomes dominant at the end phase of training. This leads to noisy results with perceivable artifacts. We show two randomly selected examples of using and not using adversarial loss annealing in Fig. 8 From the qualitative comparison, we observe that using adversarial loss annealing not only reduces the noise level but does not sacrifice the overall sharpness and local details.

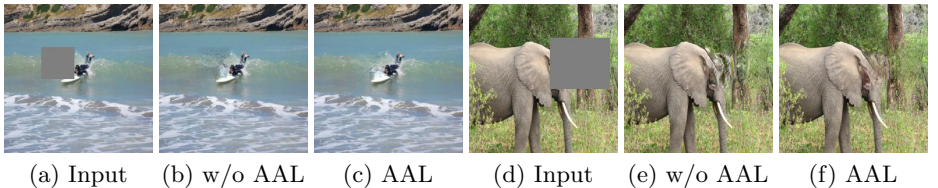


**Fig. 8.** Result comparison between training without AAL and with AAL.

**Comparing Patch Perceptual Losses with  $\ell_2$**  We compare the quality of inpainting that is trained with patch perceptual loss and  $\ell_2$  loss.  $\ell_2$  is used to train CE and GLI, but it does not correspond well to human perception of similarity, as discussed in Sec. 3.3. We investigate how our Patch Perceptual Loss compares with  $\ell_2$  loss by training the same network and only using different reconstruction loss. From the test cases, we see that our results are overwhelmingly better than  $\ell_2$  results in terms of sharpness and coherence with context. We leave detailed discussion of training losses to Supplementary Materials.



**Fig. 9.** Effects of different types of reconstruction losses. Zoom in for best quality.

#### 4.4 Interactive Guided Inpainting

Guided inpainting refers to the task of using another image as guidance to fill in the missing part of the original image. This is extremely useful in practice as people often want to add new objects or replace sceneries. It can also fill in large holes, which is a challenging task without using another image to guide. Interactive guided inpainting allows the user to freely choose the guide image and region of interest.

Here we consider the scenario of object-based guided inpainting. Specifically, we assume the user would like to add to the input image with objects from another guide image. Given an input image  $I$  and a guide image  $I_g$ , we allow the user to select a region of  $I_s$  by dragging a bounding box  $B_g$  containing the object that he desires to add. Note that unlike previous settings of image composition, we do not require the user to accurately segment the object, but instead only providing a bounding box is sufficient. This greatly reduces the workload and simplifies the task. Next, we perform segmentation use a network to extract the object foreground. The segmentation network is adapted from Mask R-CNN [51]

and trained on COCO, but is agnostic to object categories and only considers the foreground/background classification. Finally, we resize and paste  $B_g$  to  $I$ . To make the composition look natural and realistic, we need to inpaint the background of  $B$  and also perform harmonization on object foreground, such that its appearance is compatible with  $I$ .

To accomplish this task, we need to address two separate problems: inpainting and harmonization. Our model can be easily extended to train for both tasks at the same time, only requiring changing the input and output. Our data acquisition is similar to [9]. Specifically, at each iteration given the input image  $I$ , we randomly select another image  $I_g$  from the dataset. We then select and segment an object  $I_o$  from  $I$ , based on the segmentation mask of COCO. We then transfer the color from  $I_g$  to  $I_o$ , and paste  $I_o$  onto  $I_g$  at a random location. Finally, we crop a bounding box  $I_b$  from  $I_g$  that contains  $I_o$ , and paste  $I_b$  back to  $I$ . The result, together with the foreground/background segmentation mask of  $I_b$ , is given to the network as input. The model is modified to output two images, one for inpainting result and the other for harmonization result. We use the original  $I$  as the ground truth for both tasks.

The network jointly trained for inpainting and harmonization performs well in both tasks. Fig. 10 shows that it adjusts the color better than [9], which is the state-of-the-art deep harmonization method. Fig. 11 shows the interactive guided inpainting results.

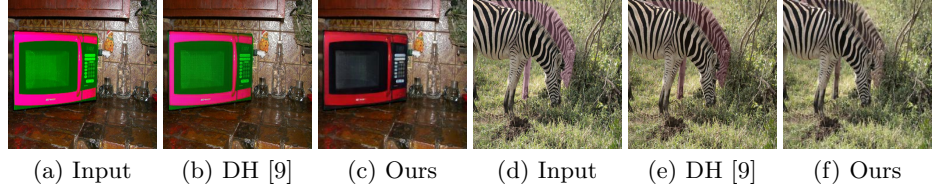


**Fig. 10.** Examples of image harmonization results. For (a) and (d), the microwave and the zebra on the back have unusual color. Our method is able to adjust their appearance such that they look coherent and realistic. Our harmonization results are also more natural and plausible than state-of-the-art method [9].

## 5 Conclusions

We proposed a novel model and training scheme to address the inpainting problem and achieve excellent performance on several tasks, including general inpainting, image harmonization and guided inpainting. Although we only explore the ability of our approach in image editing related tasks, we believe it is a general methodology that could be easily applied to other generative problems, such as image translation, image synthesis, etc. As future work, we plan to study the effectiveness of the proposed network and losses, and especially the procedural training scheme on a larger scope.

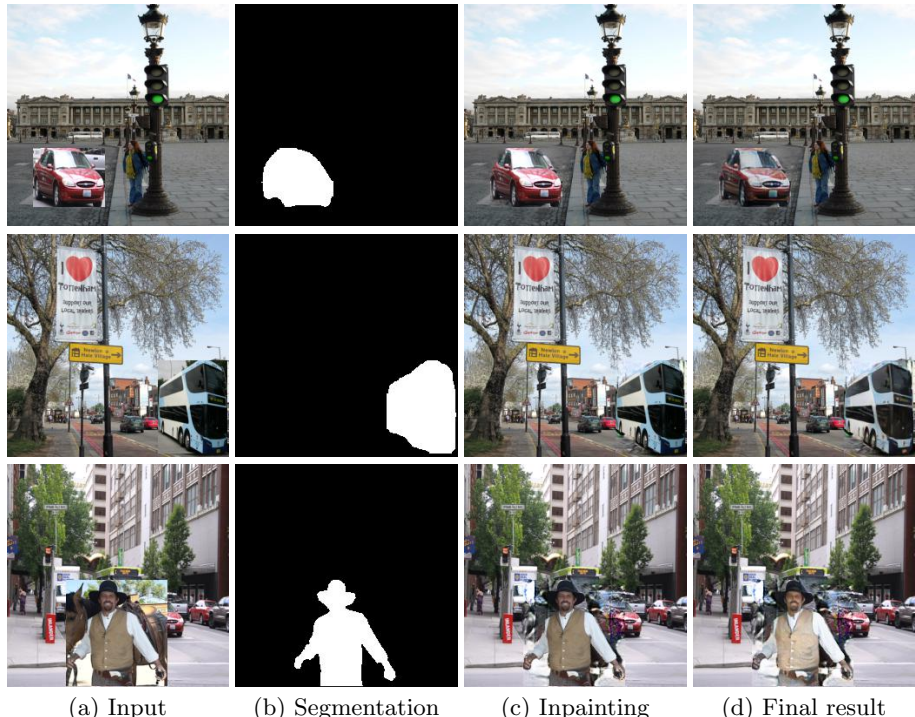


**Fig. 11.** Examples of interactive guided inpainting result. The segmentation mask is given by our foreground/background segmentation network trained on COCO. The final result combines the outputs of harmonization and inpainting.

## 855 References

- 856 1. Gatys, L., Ecker, A.S., Bethge, M.: Texture synthesis using convolutional neural  
857 networks. In: Advances in Neural Information Processing Systems. (2015) 262–270
- 858 2. Komodakis, N.: Image completion using global optimization. In: Computer Vision  
859 and Pattern Recognition, 2006 IEEE Computer Society Conference on. Volume 1.,  
860 IEEE (2006) 442–452
- 861 3. Hays, J., Efros, A.A.: Scene completion using millions of photographs. In: ACM  
862 Transactions on Graphics (TOG). Volume 26., ACM (2007) 4
- 863 4. Bertalmio, M., Sapiro, G., Caselles, V., Ballester, C.: Image inpainting. In: Pro-  
864 ceedings of the 27th annual conference on Computer graphics and interactive tech-  
865 niques, ACM Press/Addison-Wesley Publishing Co. (2000) 417–424
- 866 5. Wexler, Y., Shechtman, E., Irani, M.: Space-time video completion. In: Computer  
867 Vision and Pattern Recognition, 2004. CVPR 2004. Proceedings of the 2004 IEEE  
868 Computer Society Conference on. Volume 1., IEEE (2004) I–I
- 869 6. Barnes, C., Shechtman, E., Finkelstein, A., Goldman, D.B.: Patchmatch: A ran-  
870 domized correspondence algorithm for structural image editing. ACM Transactions  
871 on Graphics-TOG **28**(3) (2009) 24
- 872 7. Bertalmio, M., Vese, L., Sapiro, G., Osher, S.: Simultaneous structure and texture  
873 image inpainting. IEEE transactions on image processing **12**(8) (2003) 882–889
- 874 8. Wilczkowiak, M., Brostow, G.J., Tordoff, B., Cipolla, R.: Hole filling through pho-  
875 tomontage. In: BMVC 2005-Proceedings of the British Machine Vision Conference  
876 2005. (2005)
- 877 9. Tsai, Y.H., Shen, X., Lin, Z., Sunkavalli, K., Lu, X., Yang, M.H.: Deep image  
878 harmonization. In: IEEE Conference on Computer Vision and Pattern Recognition  
(CVPR). (2017)
- 879 10. Iizuka, S., Simo-Serra, E., Ishikawa, H.: Globally and locally consistent image  
880 completion. ACM Transactions on Graphics (TOG) **36**(4) (2017) 107
- 881 11. Pathak, D., Krahenbuhl, P., Donahue, J., Darrell, T., Efros, A.A.: Context en-  
882 coders: Feature learning by inpainting. In: Proceedings of the IEEE Conference on  
883 Computer Vision and Pattern Recognition. (2016) 2536–2544
- 884 12. Yeh, R., Chen, C., Lim, T.Y., Hasegawa-Johnson, M., Do, M.N.: Semantic image  
885 inpainting with perceptual and contextual losses. arXiv preprint arXiv:1607.07539  
(2016)
- 886 13. Li, Y., Liu, S., Yang, J., Yang, M.H.: Generative face completion. In: Proceedings  
887 of the IEEE Conference on Computer Vision and Pattern Recognition. Volume 1.  
888 (2017) 6
- 889 14. Yang, C., Lu, X., Lin, Z., Shechtman, E., Wang, O., Li, H.: High-resolution image  
890 inpainting using multi-scale neural patch synthesis. In: The IEEE Conference on  
891 Computer Vision and Pattern Recognition (CVPR). Volume 1. (2017) 3
- 892 15. Zhang, R., Isola, P., Efros, A.A., Shechtman, E., Wang, O.: The unreasonable effec-  
893 tiveness of deep features as a perceptual metric. arXiv preprint arXiv:1801.03924  
(2018)
- 894 16. Johnson, J., Alahi, A., Fei-Fei, L.: Perceptual losses for real-time style transfer and  
895 super-resolution. In: European Conference on Computer Vision, Springer (2016)  
896 694–711
- 897 17. Gatys, L.A., Ecker, A.S., Bethge, M.: Image style transfer using convolutional  
898 neural networks. In: Computer Vision and Pattern Recognition (CVPR), 2016  
899 IEEE Conference on, IEEE (2016) 2414–2423

- 900 18. Dosovitskiy, A., Brox, T.: Generating images with perceptual similarity metrics  
901 based on deep networks. In: Advances in Neural Information Processing Systems.  
902 (2016) 658–666
- 903 19. Chen, Q., Koltun, V.: Photographic image synthesis with cascaded refinement  
904 networks. In: The IEEE International Conference on Computer Vision (ICCV).  
905 Volume 1. (2017)
- 906 20. Goodfellow, I., Pouget-Abadie, J., Mirza, M., Xu, B., Warde-Farley, D., Ozair, S.,  
907 Courville, A., Bengio, Y.: Generative adversarial nets. In: Advances in neural  
908 information processing systems. (2014) 2672–2680
- 909 21. Denton, E.L., Chintala, S., Fergus, R., et al.: Deep generative image models using  
910 a laplacian pyramid of adversarial networks. In: Advances in neural information  
911 processing systems. (2015) 1486–1494
- 912 22. Radford, A., Metz, L., Chintala, S.: Unsupervised representation learning  
913 with deep convolutional generative adversarial networks. arXiv preprint  
914 arXiv:1511.06434 (2015)
- 915 23. Zhao, J., Mathieu, M., LeCun, Y.: Energy-based generative adversarial network.  
916 arXiv preprint arXiv:1609.03126 (2016)
- 917 24. Arjovsky, M., Chintala, S., Bottou, L.: Wasserstein gan. arXiv preprint  
918 arXiv:1701.07875 (2017)
- 919 25. Gulrajani, I., Ahmed, F., Arjovsky, M., Dumoulin, V., Courville, A.: Improved  
920 training of wasserstein gans. arXiv preprint arXiv:1704.00028 (2017)
- 921 26. Karras, T., Aila, T., Laine, S., Lehtinen, J.: Progressive growing of gans for im-  
922 proved quality, stability, and variation. arXiv preprint arXiv:1710.10196 (2017)
- 923 27. Kim, J., Kwon Lee, J., Mu Lee, K.: Accurate image super-resolution using very  
924 deep convolutional networks. In: Proceedings of the IEEE Conference on Computer  
925 Vision and Pattern Recognition. (2016) 1646–1654
- 926 28. Dong, C., Loy, C.C., He, K., Tang, X.: Learning a deep convolutional network for  
927 image super-resolution. In: European Conference on Computer Vision, Springer  
928 (2014) 184–199
- 929 29. Ledig, C., Theis, L., Huszár, F., Caballero, J., Cunningham, A., Acosta, A., Aitken,  
930 A., Tejani, A., Totz, J., Wang, Z., et al.: Photo-realistic single image super-  
931 resolution using a generative adversarial network. arXiv preprint arXiv:1609.04802  
932 (2016)
- 933 30. Isola, P., Zhu, J.Y., Zhou, T., Efros, A.A.: Image-to-image translation with con-  
934 ditional adversarial networks. arXiv preprint arXiv:1611.07004 (2016)
- 935 31. Zhu, J.Y., Park, T., Isola, P., Efros, A.A.: Unpaired image-to-image translation us-  
936 ing cycle-consistent adversarial networks. arXiv preprint arXiv:1703.10593 (2017)
- 937 32. Wang, T.C., Liu, M.Y., Zhu, J.Y., Tao, A., Kautz, J., Catanzaro, B.: High-  
938 resolution image synthesis and semantic manipulation with conditional gans. arXiv  
939 preprint arXiv:1711.11585 (2017)
- 940 33. Zhu, J.Y., Krähenbühl, P., Shechtman, E., Efros, A.A.: Learning a discriminative  
941 model for the perception of realism in composite images. In: Computer Vision  
942 (ICCV), 2015 IEEE International Conference on. (2015)
- 943 34. Elad, M., Starck, J.L., Querre, P., Donoho, D.L.: Simultaneous cartoon and texture  
944 image inpainting using morphological component analysis (mca). Applied and  
945 Computational Harmonic Analysis **19**(3) (2005) 340–358
- 946 35. Reinhard, E., Adhikhmin, M., Gooch, B., Shirley, P.: Color transfer between im-  
947 ages. IEEE Computer graphics and applications **21**(5) (2001) 34–41
- 948 36. Sunkavalli, K., Johnson, M.K., Matusik, W., Pfister, H.: Multi-scale image har-  
949 monization. In: ACM Transactions on Graphics (TOG). Volume 29., ACM (2010)  
950 125

- 945 37. Pérez, P., Gangnet, M., Blake, A.: Poisson image editing. ACM Transactions on  
946 graphics (TOG) **22**(3) (2003) 313–318  
947 38. Tao, M.W., Johnson, M.K., Paris, S.: Error-tolerant image compositing. In: European  
948 Conference on Computer Vision, Springer (2010) 31–44  
949 39. Tsai, Y.H., Shen, X., Lin, Z., Sunkavalli, K., Yang, M.H.: Sky is not the limit:  
950 semantic-aware sky replacement. ACM Trans. Graph. **35**(4) (2016) 149–1  
951 40. Johnson, M.K., Dale, K., Avidan, S., Pfister, H., Freeman, W.T., Matusik, W.:  
952 Cg2real: Improving the realism of computer generated images using a large collec-  
953 tion of photographs. IEEE Transactions on Visualization and Computer Graphics  
954 **17**(9) (2011) 1273–1285  
955 41. Mirza, M., Osindero, S.: Conditional generative adversarial nets. arXiv preprint  
956 arXiv:1411.1784 (2014)  
957 42. He, K., Zhang, X., Ren, S., Sun, J.: Deep residual learning for image recognition.  
958 In: Proceedings of the IEEE conference on computer vision and pattern recognition.  
959 (2016) 770–778  
960 43. Yu, F., Koltun, V.: Multi-scale context aggregation by dilated convolutions. arXiv  
961 preprint arXiv:1511.07122 (2015)  
962 44. Odena, A., Dumoulin, V., Olah, C.: Deconvolution and checkerboard artifacts.  
963 Distill (2016)  
964 45. Zhang, H., Xu, T., Li, H., Zhang, S., Huang, X., Wang, X., Metaxas, D.: Stack-  
965 gan: Text to photo-realistic image synthesis with stacked generative adversarial  
966 networks. arXiv preprint arXiv:1612.03242 (2016)  
967 46. Durugkar, I., Gemp, I., Mahadevan, S.: Generative multi-adversarial networks.  
968 arXiv preprint arXiv:1611.01673 (2016)  
969 47. Lin, T.Y., Maire, M., Belongie, S., Hays, J., Perona, P., Ramanan, D., Dollár, P.,  
970 Zitnick, C.L.: Microsoft coco: Common objects in context. In: European conference  
971 on computer vision, Springer (2014) 740–755  
972 48. Zhou, B., Khosla, A., Lapedriza, A., Torralba, A., Oliva, A.: Places: An image  
973 database for deep scene understanding. arXiv preprint arXiv:1610.02055 (2016)  
974 49. Ziwei Liu, Ping Luo, X.W., Tang, X.: Deep learning face attributes in the wild.  
975 In: Proceedings of International Conference on Computer Vision (ICCV). (2015)  
976 50. Russakovsky, O., Deng, J., Su, H., Krause, J., Satheesh, S., Ma, S., Huang, Z.,  
977 Karpathy, A., Khosla, A., Bernstein, M., et al.: Imagenet large scale visual recog-  
978 nition challenge. International Journal of Computer Vision **115**(3) (2015) 211–252  
979 51. He, K., Gkioxari, G., Dollár, P., Girshick, R.: Mask r-cnn. In: Computer Vision  
980 (ICCV), 2017 IEEE International Conference on, IEEE (2017) 2980–2988  
981  
982  
983  
984  
985  
986  
987  
988  
989